

# Confined Water in Layered Silicates: The Origin of Anomalous Thermal Expansion Behavior in Calcium-Silicate-Hydrates

N. M. Anoop Krishnan,<sup>†,‡,§,||</sup> Bu Wang,<sup>†,‡,§</sup> Gabriel Falzone,<sup>†</sup> Yann Le Pape,<sup>§</sup> Narayanan Neithalath,<sup>||</sup> Laurent Pilon,<sup>⊥</sup> Mathieu Bauchy,<sup>\*,‡</sup> and Gaurav Sant<sup>\*,†,#</sup>

<sup>†</sup>Laboratory for the Chemistry of Construction Materials (LC<sup>2</sup>), Department of Civil and Environmental Engineering, University of California, Los Angeles, California 90095, United States

<sup>‡</sup>Laboratory for the Physics of Amorphous and Inorganic Solids (PARISlab), Department of Civil and Environmental Engineering, University of California, Los Angeles, California 90095, United States

<sup>§</sup>Oak Ridge National Laboratory, P.O. Box 2008, Oak Ridge, Tennessee 37831, United States

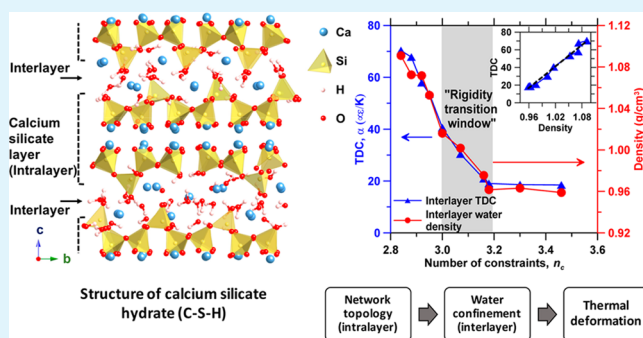
<sup>||</sup>School of Sustainable Engineering and the Built Environment, Arizona State University, Tempe, Arizona 85281, United States

<sup>⊥</sup>Department of Mechanical and Aerospace Engineering, University of California, Los Angeles, California 90095, United States

<sup>#</sup>California Nanosystems Institute (CNSI), University of California, Los Angeles, California 90095, United States

**ABSTRACT:** Water, under conditions of nanoscale confinement, exhibits anomalous dynamics, and enhanced thermal deformations, which may be further enhanced when such water is in contact with hydrophilic surfaces. Such heightened thermal deformations of water could control the volume stability of hydrated materials containing nanoconfined structural water. Understanding and predicting the thermal deformation coefficient (TDC, often referred to as the CTE, coefficient of thermal expansion), which represents volume changes induced in materials under conditions of changing temperature, is of critical importance for hydrated solids including: hydrogels, biological tissues, and calcium silicate hydrates, as changes in their volume can result in stress development, and cracking. By pioneering atomistic simulations, we examine the physical origin of thermal expansion in calcium-silicate-hydrates (C–S–H), the binding agent in concrete that is formed by the reaction of cement with water. We report that the TDC of C–S–H shows a sudden increase when the CaO/SiO<sub>2</sub> (molar ratio; abbreviated as Ca/Si) exceeds 1.5. This anomalous behavior arises from a notable increase in the confinement of water contained in the C–S–H's nanostructure. We identify that confinement is dictated by the topology of the C–S–H's atomic network. Taken together, the results suggest that thermal deformations of hydrated silicates can be altered by inducing compositional changes, which in turn alter the atomic topology and the resultant volume stability of the solids.

**KEYWORDS:** silicates, thermal expansion, atomistic simulation, topology, confinement



## 1. INTRODUCTION AND BACKGROUND

It is well-known that water under confinement at the nanoscale features drastically different characteristics from bulk water.<sup>1–7</sup> The behavior of such *nanoconfined water* is of fundamental importance to understand biological activity in living cells,<sup>8</sup> and it also gives rise to unique properties in other materials, including: enhanced mechanical properties of spider silk,<sup>9</sup> reactivity of organic materials,<sup>10</sup> energy storage applications,<sup>11</sup> and increased heat capacity of porous glasses.<sup>12</sup> As such it appears possible to design material systems containing nanoconfined water to achieve targeted properties by enhancing or suppressing such confinement. For example, in a layered solid such as C–S–H, this could be accomplished by changing the interlayer spacing within which water molecules are confined. Herein, a decrease in the interlayer spacing results in an increase in the confinement of water. Somewhat analogously, confining water between very highly hydrophilic

solid surfaces has been proposed as a potential pathway for enhancing the thermal conductivity of thermal interface materials.<sup>7</sup>

Tuning the confinement of water at the solid–fluid interface requires critical understanding of how the underlying solid, and its atomic structure impose confinement. To secure such insight previous studies have examined the confinement of water by hydrophilic silicate structures, such as quartz, silica and other silicate minerals.<sup>2,6,7,13</sup> Particularly, nanoconfined water in layered silicates, such as mica and calcium silicate hydrates (C–S–H) has received substantial attention.<sup>1,4,13,14</sup> These studies have revealed that the water confined in the silicate network of C–S–H exhibits characteristics reminiscent of a glassy

**Received:** September 13, 2016

**Accepted:** December 6, 2016

**Published:** December 6, 2016

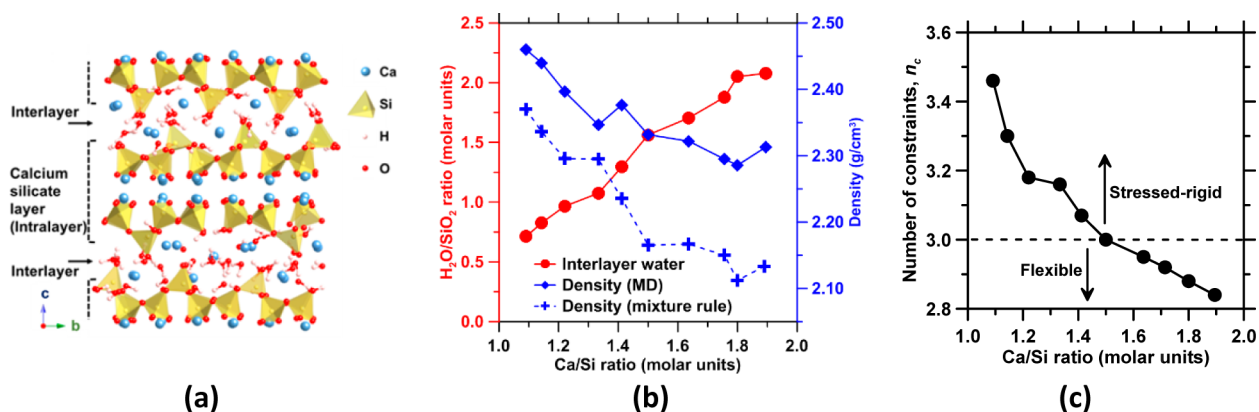


**Figure 1.** (a) Representative C–S–H structure for Ca/Si = 1.1, showing the interlayer and intralayer domains. (b) C–S–H density (i.e., corresponding to C–S–H free of pore water, porosity, portlandite, etc.) and H<sub>2</sub>O content of C–S–H’s across a range of compositions of general formula, (CaO)<sub>x</sub>(SiO<sub>2</sub>)(H<sub>2</sub>O)<sub>y</sub>, predicted via MD simulations and a rule of mixtures (see eq 1). (c) The variation in the number of constraints per atom ( $n_c$ , unitless) for a range of C–S–H compositions as a function of Ca/Si.

compound.<sup>4</sup> Further, for certain compositions, nanoconfined water in C–S–H exhibits anomalous dynamics.<sup>3</sup> Such anomalous behavior can result in changes in thermal deformation behavior, which can have significant practical implications. For example, C–S–H, serves as the main binding agent present in concrete formed from the reaction of ordinary portland cement (OPC) with water.<sup>15,16</sup> Controlling the thermal behavior of such solids via compositional design is important to prevent the degradation of constructed facilities resulting from excessive thermal deformations and cracking. While it is anecdotally known that changes in composition can induce changes in the disorder of the atomic network of C–S–H,<sup>3,15,17</sup> the influences on confinement, if any, remains poorly understood.

Therefore, we investigate the nanoconfinement and thermal deformation behavior for a range of C–S–H compositions with  $1.1 \leq \text{Ca/Si} \leq 1.9$  via molecular dynamics (MD) simulations. To fully elucidate the effects of composition, special efforts are made to isolate the influences, and the importance of the role of water content, the extent of silicate structure depolymerization, and of interlayer spacing. We find that, in layered hydrated silicates, such as C–S–H, the interlayer water dictates thermal deformation behavior, as a function of its increasing confinement. The extent of confinement of such water shows a distinct compositional dependence, which is rooted in the alteration of the silicate layer-water interface topology. Significantly, as an increase in Ca/Si ratio induces a topological transition in the silicate network from rigid to flexible, a strong interface relaxation, accompanied by an anomalous jump in the thermal deformation coefficient (TDC), is observed. These atomistic insights into the composition-dependent confinement of water help clarify pathways to synthesize novel materials with desirable thermal properties.

## 2. COMPUTATIONAL METHODOLOGY

**2.a. Structure of C–S–H.** C–S–H has a layered structure consisting of (i) intralayer domains, which consist of calcium-silicate networks, and (ii) interlayer domains which contain water molecules, OH<sup>−</sup> and Ca<sup>2+</sup> ions (Figure 1a). The intralayer calcium-silicate network exhibits well-defined short-range order ( $\sim 2$  Å, which includes the calcium-silicate framework comprising silicon tetrahedra and Ca–O bonds). But, at the “long-range” ( $>10$  Å), the extent of disorder increases with Ca/Si. For example, the substrate C–S–H structures with Ca/Si < 1.5 are reminiscent of their crystalline analogue,

tobermorite. This is seen in the calcium-silicate framework which is not amorphous and structurally differs from a glassy network.<sup>18</sup> However, at higher Ca/Si ratios, the substrates show a disordered glass-like network at the long-range order, while still retaining the layered structure similar to tobermorite. The interlayer spacing increases with Ca/Si as the structure exhibits increasing disorder.<sup>3</sup>

To study the compositional dependence of thermal deformations, the C–S–H model developed by Pellenq et al.<sup>17,19</sup> was used. This model was used to generate the C–S–H structures for  $1.1 \leq \text{Ca/Si} \leq 1.9$ . These structures were constructed from a (parent) 11 Å tobermorite structure by randomly removing charge-neutral SiO<sub>2</sub> (ref 17, see Figure 1a) to achieve a wide-range of Ca/Si ratios. These structures are consistent with the stoichiometry of C–S–H that is assessed by small-angle neutron scattering (SANS). Moreover, these structures also reproduce structural features such as pair distribution functions (PDFs), IR spectra, and mechanical properties as assessed experimentally.<sup>17</sup> Figure 1b shows the variation of density and water content of these structures as a function of Ca/Si molar ratio. The water content increases with Ca/Si, resulting in a decrease in the density.<sup>15</sup>

The C–S–H model used herein has been subjected to substantial scrutiny and several outstanding issues have been identified.<sup>20–22</sup> First, the density of C–S–H predicted by the model differs from experiments; which is thought to be on account of differences in cell volumes,<sup>20</sup> and a lack of relaxation of the model structure.<sup>23</sup> However, qualitatively the trend in the density versus Ca/Si ratio relation is similar to experimental data.<sup>20</sup> This trend is further confirmed using a simple rule of mixtures, where the density of C<sub>x</sub>–S<sub>y</sub>–H<sub>y</sub>,  $\rho_{\text{C-S-H}}$ , is expressed in terms of the mole fractions of its simple oxide constituents as a mechanical mixture

$$\rho_{\text{C-S-H}} = \frac{x\rho_{\text{C}} + \rho_{\text{S}} + y\rho_{\text{H}}}{1 + x + y} \quad (1)$$

where  $\rho_{\text{C}}$ ,  $\rho_{\text{S}}$ , and  $\rho_{\text{H}}$  are the densities of CaO (C), SiO<sub>2</sub> (S), and H<sub>2</sub>O (H), respectively and  $x$  and  $y$  are the mole fractions of C and H per unit mole of S. The densities of the individual components are obtained from the literature to be  $\rho_{\text{H}} = 1$  g/cm<sup>3</sup>,<sup>24</sup>  $\rho_{\text{S}} = 2.2$  g/cm<sup>3</sup>,<sup>24</sup>  $\rho_{\text{C}} = 3.34$  g/cm<sup>3</sup>.<sup>24</sup> The density predicted from the mixture rule is shown in Figure 1b, where the overall trend is in agreement with densities predicted from MD simulations. Second, the model of Pellenq et al.<sup>17,19</sup> predicts the presence of Q<sup>0</sup> (i.e., an isolated, uncoordinated silicate anion) units which have not been observed in C–S–H. As such, the calcium silicate network in the model, particular at high Ca/Si, is expected to be overly depolymerized. The potential effects of these discrepancies on the results are discussed where relevant.

**2.b. Molecular Dynamics Simulation.** Molecular dynamics (MD) simulations were carried out on 10 distinct C–S–H compositions using the large-scale atomic/molecular massively parallel

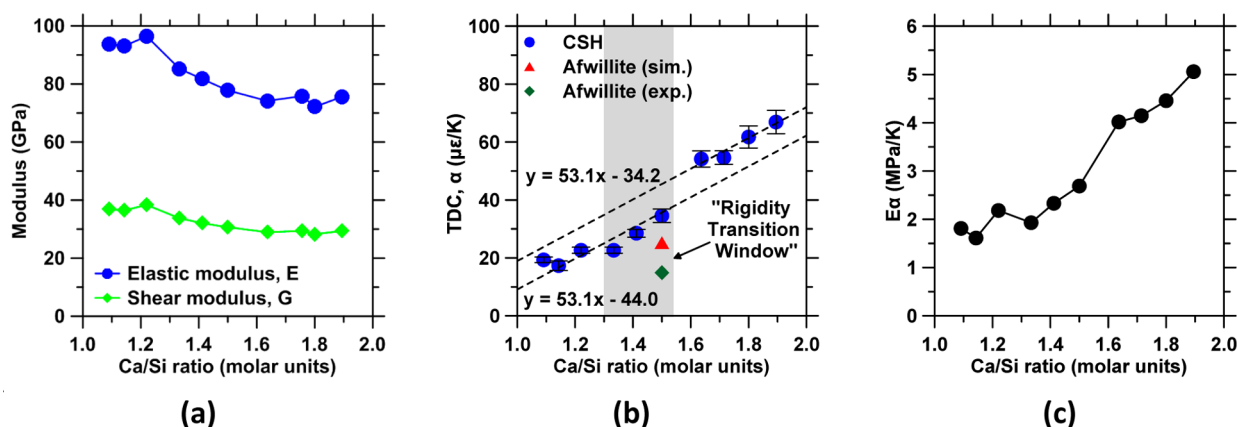


**Figure 2.** (a) Elastic ( $E$ ) and shear ( $G$ ) moduli of C–S–H as a function of Ca/Si. (b) Linearized (i.e., assuming isotropy) TDC ( $\alpha$ ) of the C–S–H compositions as a function of Ca/Si. Also shown are the experimental (exp.) and simulated (sim.) TDC's of the crystalline C–S–H mineral afwillite (Ca/Si = 1.5). The TDC shows a “jump” across the rigidity transition window (shaded). (c) The elastic thermal stress ( $E\alpha$ ) developed in C–S–H for a unit change in temperature, calculated as the product of elastic modulus and the TDC.

simulator (LAMMPS).<sup>25</sup> The interactions between the atoms were modeled using the CSH-FF interatomic potential,<sup>26</sup> a variant of the ClayFF potential that is parametrized for C–S–H systems.<sup>19</sup> This potential has been calibrated using mechanical and structural properties, for example, elastic modulus and lattice parameters of the crystalline C–S–H mineral, tobermorite. CSH-FF represents water molecules using the flexible simple point charge (SPC) model<sup>27</sup> with partial charges associated with O and H as  $-0.82$  and  $0.41$ , respectively. Thus, the dynamics of water molecules are reasonably described by CSH-FF, with the ability to simulate solid–water interactions. The details of the other partial charges on other atoms and other relevant parameters can be found elsewhere.<sup>26</sup>

The system was first equilibrated at 333 K for 200 ps. Using a time-step of 1 fs Newton's equations of motion were integrated using the velocity-Verlet scheme. Equilibrium properties, including the molar volume, and temperature, were obtained by running the simulations for another 100 ps while averaging the volume and cell size over the entire 100 ps duration. Then, the system was cooled by 10 K, at the rate of 1 K/ps. The system was equilibrated at this temperature and the equilibrium properties were obtained. This process was continued until a temperature of 283 K was achieved. As such, the simulations encompassed a temperature range from 10 °C to 60 °C. The upper limit ensured that the water present in C–S–H does not undergo any phase change.<sup>28,29</sup> The linear thermal deformation coefficient ( $\alpha$ , TDC,  $\mu\epsilon/K$ ) of C–S–H assuming isotropic behavior was calculated as

$$\alpha \approx \frac{1}{3\Delta T} \left( \frac{\Delta V}{V} \right) \quad (2)$$

where  $\Delta V/V$  is the volumetric strain ( $\mu\epsilon$ ) and  $\Delta T$  is the change in temperature (K). A least-squares fit was used to obtain the slope of the  $[V-T]$  diagram to obtain the TDC. Each simulation was repeated six times to assess the uncertainty in the MD results. To elucidate the mechanisms of thermal expansion in detail, Voronoi tessellations were carried out on equilibrium structures. The Voronoi volumes were used to calculate the Voronoi density of interlayer water molecules, which indicate the extent to which water was confined in the C–S–H structure. Further, the contribution of this confined interlayer water on the TDC was evaluated separately, that is, by calculating their respective Voronoi volumes and the associated TDCs. Furthermore, the elastic properties of the C–S–H compositions were assessed. To calculate the elastic tensors of each C–S–H composition, a small strain of  $\epsilon = \pm 0.01$  was applied along the respective principle directions in steps of  $\epsilon = \pm 0.001$ . Energy minimization was performed using a conjugate-gradient algorithm to obtain the converged values of the stresses and the respective components of the elastic tensor. For each composition, the effective elastic and shear moduli were calculated using this tensor.

**2.c. Topological Constraints in C–S–H.** To elucidate the effect of the calcium silicate network on the confinement of water and thermal expansions topological constraint theory (TCT) was applied.<sup>30</sup> TCT offers a means to reduce a complex atomic network into an equivalent mechanical truss, with the nodes representing atoms and the rigid bars (i.e., members) representing chemical bonds. By analogy to Maxwell's stability criteria,<sup>31</sup> it is proposed in TCT that the atomic network is isostatic (i.e., statically determinate) when the number of constraints per atom,  $n_c$ , in the atomic network is equal to the number of degrees of freedom, that is, three in 3-D. In turn,  $n_c < 3$  represents a flexible network (a hypostatic truss) that allows for internal rearrangements, and  $n_c > 3$  represents a stressed-rigid network (i.e., hyperstatic truss). TCT enables robust analysis of disordered atomic networks and has been applied to predict composition dependent properties such as hardness<sup>32</sup> and viscosity<sup>33</sup> of silicate glasses and C–S–H.<sup>34</sup> TCT has also been previously applied to identify composition induced rigidity transitions in C–S–H.<sup>35</sup> As such, constraint enumeration is carried out using MD simulations to characterize both broken and intact constraints by evaluating the extent of radial and angular excursions, that is, for bond-stretching (BS) and bond-bending (BB) constraints, respectively. This method has been applied for both chalcogenide<sup>36</sup> and silicate glasses.<sup>37</sup> For C–S–H, substantial differences in the standard deviations between intact and broken constraints ( $\geq 10\%$ ) are observed, thus allowing them to be unambiguously distinguished.<sup>35</sup>

### 3. RESULTS AND DISCUSSIONS

**3.a. Elastic Modulus.** First, the number of constraints assessed for each C–S–H composition is shown in Figure 1c. In general, the C–S–H's rigidity decreases with increasing calcium and water content, that is, increasing Ca/Si.<sup>35</sup> Isostatic compositions ( $n_c \approx 3$ ) are identified for  $1.3 \leq \text{Ca/Si} \leq 1.5$ . When Ca/Si > 1.5, the structures are flexible, and tolerate local rearrangements of their network. For Ca/Si < 1.3, the structures are stressed-rigid and show little if any ability for local rearrangement.

Second, the assessed elastic  $E$  and the shear  $G$  moduli of the different C–S–H compositions were plotted as a function of Ca/Si as shown in Figure 2a. It should be noted that the C–S–H systems with low Ca/Si ratios exhibit some transverse isotropy, while systems with Ca/Si  $\geq 1.5$  are more isotropic. The elastic and shear moduli decrease as Ca/Si increases, as noted experimentally for the indentation modulus, indentation hardness and fracture toughness.<sup>17,34,38,39</sup> This is because an increase in the Ca-content depolymerizes the intralayer silicate

network while simultaneously increasing the interlayer water content, both of which weaken the C–S–H structure. This induces a “composition-dependent softening”. At this point, however, the origin of the composition linked softening is not fully clear, and more in-depth study is yet needed.

**3.b. Thermal Deformation Coefficient (TDC).** Figure 2b shows the TDC of the different C–S–H compositions. As Ca/Si molar ratio increases, so does the TDC. This is in contrast to the elastic moduli, which decrease with increasing Ca/Si ratio. While it may be presumed that simultaneously reducing the stiffness and increasing the TDC with increasing Ca/Si may counterbalance each other in terms of thermal stress development—this is not so. In fact, the more significant increase in the TDC with Ca/Si ensures that the elastic thermal stress,  $E\alpha$ , developed increases with Ca/Si ratio (e.g., see Figure 2c) ensuring that, practically, the risk of thermal cracking would amplify proportionately.

At this point, it should be noted that the TDC values shown in Figure 2b correspond to that of pure C–S–H compounds. That said, no contributions of the pore water, portlandite, and the other hydrates (e.g., AFm, AFt, etc.<sup>40</sup>) are included. Further, while the calculated TDC's are similar to measured data for low Ca/Si, the MD-calculated TDC's are 3–6 times larger than the measured TDC of a hardened cement paste  $\sim 10$ -to- $20 \mu\text{E}/\text{K}$ <sup>41,42</sup> – for compositions that contain  $>50$  mass % C–S–H with Ca/Si  $\approx 1.8$ . This discrepancy is thought to arise because interatomic potentials are parametrized to equilibrium properties, and are thus unable to accurately capture anharmonic contributions that result from thermal excitations, unless specifically parametrized.<sup>43</sup> Thus, to evaluate the effects of interatomic potential choice on the simulation, the TDC of afwillite, a crystalline C–S–H mineral with Ca/Si = 1.5 was simulated. While there exist numerous other C–S–H minerals, experimental data on the TDC of these minerals is scarce; hence, afwillite is the example we focus on. Afwillite, a calcium silicate mineral ( $\text{Ca}_3(\text{SiO}_4)(\text{SiO}_2(\text{OH})_2) \cdot 2\text{H}_2\text{O}$ ) crystallizes in a monoclinic crystal system. The isolated silicon tetrahedra in afwillite share their edges with the octahedra formed by the interstitial calcium atoms and the neighboring oxygen atoms. The MD-calculated TDC of afwillite is around two times larger than the measured value, as illustrated in Figure 2b.<sup>44</sup> Since the temperature dependence of material properties were not explicitly considered when the CSH-FF potential was parametrized,<sup>19</sup> such mismatch is not unexpected.<sup>43</sup> Thus, it can be assumed that the MD-calculated TDC for all the C–S–H compositions is associated with a similar level of overestimation. This issue is yet further complicated when considering interatomic potentials for water, for example, the SPC model too overestimates the TDC of water whose contributions are increasingly significant with increasing Ca/Si.<sup>45</sup>

The increase of TDC with Ca/Si ratio is expected, since the water content increases with Ca/Si (Figure 1b), and water exhibits greater thermal expansion than an oxide solid in the temperature range of interest.<sup>45–48</sup> However, the water content and TDC trends as a function of Ca/Si ratio show differing trends. For example, as shown in Figure 1b, the dependence of water content on Ca/Si ratio is significant when Ca/Si  $\leq 1.5$ , but becomes less so in the high Ca/Si region (i.e., which shows a lower slope). On the contrary, the TDC's of C–S–H compositions lying below and above Ca/Si  $\approx 1.5$  show similar slopes, that is, the same rate of change of TDC for a unit increase in Ca/Si ratio. Significantly, for Ca/Si  $> 1.5$ , the TDC

shows a jump on the order of  $10 \mu\text{E}/\text{K}$ . This suggests that mechanisms other than simply an increase in water content are at the origin of the composition-dependent TDC increase. Such mechanisms may include contributions from (i) the confined interlayer water whose amplified TDC (i.e., relative to that of bulk water<sup>6</sup>) could increase the thermal expansion of the C–S–H's structure and (ii) the intralayer calcium silicate structure whose depolymerization with increasing Ca-content reduces the connectivity of the network. It should be noted that the jump in the TDC occurs as the C–S–H structure undergoes a composition-induced rigidity transition from the stressed-rigid to flexible domains (Figure 1c); a point which is further discussed below.

**3.c. Effect of Composition on TDC.** To better elucidate the compositional dependence, the simulated TDC is compared with the TDC estimated by a stoichiometric (linear) rule of mixtures similar to Vegard's law<sup>49</sup> that has been used to estimate composition dependent lattice parameter alterations. Following the general formula of  $(\text{CaO})_x(\text{SiO}_2)(\text{H}_2\text{O})_y$ , the TDC of C–S–H can be estimated from mixtures of CaO (lime, TDC =  $4.5 \mu\text{E}/\text{K}$ ),<sup>48</sup>  $\text{SiO}_2$  (silica, TDC =  $0.17 \mu\text{E}/\text{K}$ )<sup>46</sup> and  $\text{H}_2\text{O}$  (bulk water, TDC =  $69 \mu\text{E}/\text{K}$ )<sup>45</sup> similar to the density estimation using eq 1. This TDC estimation is shown in Figure 3a. To account for the presence of dissociated water (i.e.,  $\text{OH}^-$

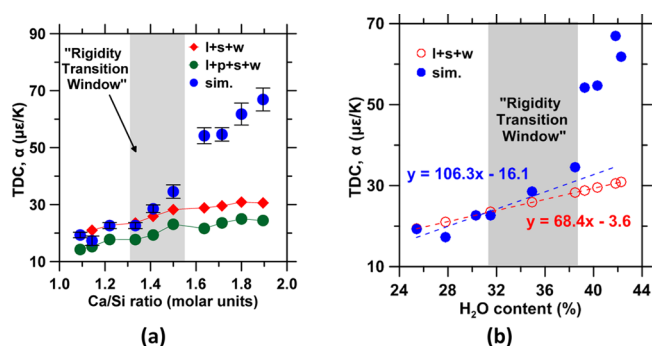


**Figure 3.** (a) TDCs of C–S–H estimated by a stoichiometric rule of mixtures. The mixture comprises lime (l), silica (s), portlandite (p), and water (w), and shown alongside are the MD simulation results (sim.) and (b) the TDC as a function of the water content. The stoichiometric rule of mixtures is noted to match simulation data below the rigidity transition window, that is, for Ca/Si  $< 1.5$ .

groups) another set of estimations were made by including  $\text{Ca}(\text{OH})_2$  (portlandite, TDC =  $19.9 \mu\text{E}/\text{K}$ )<sup>47</sup> in the mixture to account for hydroxyl groups. As shown in Figure 3a, both estimations follow similar trends—though with an offset to account for the difference in the TDC of dissociated versus bulk water; as contained in portlandite. In addition, it is important to note that both the estimated TDCs show similar trends across the entire range of Ca/Si. Significantly, while the TDC's that are estimated from a rule of mixtures are similar to the MD-calculated TDC's for Ca/Si  $\leq 1.4$ , the curves diverge dramatically at higher Ca/Si ratio.

Since the TDC of water is an order of magnitude larger than that of either lime or silica,<sup>45,46,48</sup> the thermal expansion of water is expected to be a major contributor to the TDC of C–S–H. To highlight this contribution, Figure 3b plots the TDC of C–S–H as a function of its water content. If the TDC were to simply increase with water content—the trend shown in Figure 3b should be continuous—that is, in accordance with a stoichiometric rule of mixtures. Interestingly, TDC's calculated

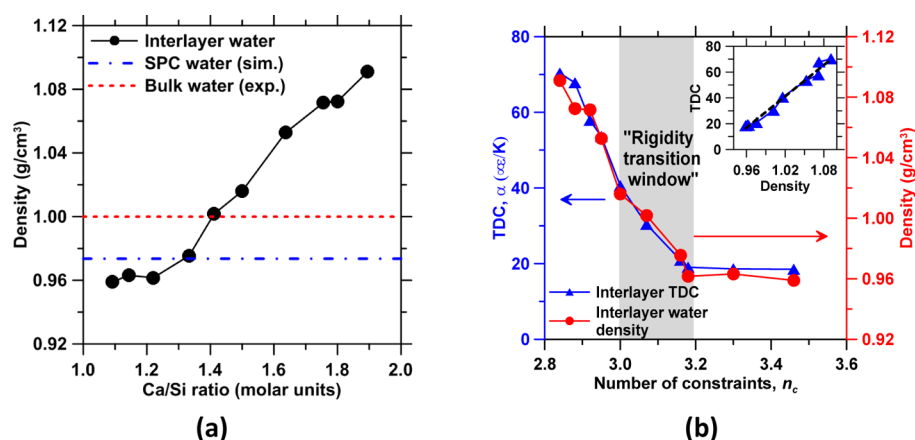


**Figure 4.** (a) Voronoi density of water molecules as a function of Ca/Si at 1 bar and 25 °C. For comparison, the density of bulk water from the MD simulations (i.e., the SPC model embedded in the CSH-FF potential), and experimental data are also shown. (b) Interlayer TDC and interlayer water density as a function of the number of constraints per atom,  $n_c$ . The inset shows the interlayer TDC as a function of the interlayer water density; quantities that follow a linear correlation shown by the dashed line.

by MD simulations follow a linear trend with the water content, but only for a water content <38% and Ca/Si  $\leq$  1.5. The slope of the MD-trend however is somewhat higher than its equivalent linear rule of mixtures approximation likely on account of overestimation of the thermal expansions of water with respect to lime, and silica by the interatomic potentials (Figure 3b). However, for Ca/Si  $\geq$  1.5, the MD-calculated TDC diverges substantially from the rule of mixtures trend. While this is in agreement with the compositional window corresponding to the rigidity transition (see Figure 1c), it suggests that the TDC of water amplifies substantially in the flexible domain, that is for Ca/Si  $\geq$  1.5 (molar ratio). Note that the composition corresponding to the rigidity transition (Ca/Si  $\approx$  1.5) is also supported experimentally by a minimum of its dissolution rate and creep compliance.<sup>23</sup> Further, these observations of the TDC, and rigidity trends appear to coincide with previous experimental observations on the existence of two different C–S–H compounds,  $\beta$ -C–S–H (1 < Ca/Si < 1.5) and  $\gamma$ -C–S–H (1.5 < Ca/Si < 2), separated around a Ca/Si ratio of 1.5.<sup>50–52</sup>

**3.d. Confinement of Water in C–S–H.** In C–S–H, water molecules are confined in interlayer positions (Figure 1a). Previous studies have shown that confined water can exhibit TDC's that are substantially larger than that of bulk water.<sup>2,6</sup> Such an increase in the TDC have been attributed to the modification of the structure of water molecules near silica surfaces. This modification is similar to that observed under conditions of increased pressure or temperature, wherein water shows increased thermal deformation. Since, the C–S–H substrate is primarily a silicate network, it is postulated that the origin of the unexpected jump in TDC with increasing Ca/Si is due to the increasing confinement of the interlayer water. To better examine this aspect, the Voronoi volume for each atom is determined from the simulated structures, allowing the density of each species to be estimated.

Figure 4a shows the Voronoi density of the interlayer water molecules at 25 °C that is estimated by averaging over all such molecules that are present. The interlayer water shows a density near-equivalent to bulk water (simulated) for Ca/Si  $\leq$  1.3 (i.e., stressed-rigid compositions) – suggesting minimal confinement. However, for Ca/Si  $\geq$  1.3 the density of the interlayer water substantially exceeds bulk water; suggesting a progressive increase in nanoscale confinement. This suggests that in the

flexible domain, the divergence of the calculated TDC, from the rule of mixtures approach (Figure 3b) is caused by the increasing contributions of confined water on the thermal deformation response.

As such, the contributions of interlayer water in the proximity of OH<sup>−</sup> groups and Ca<sup>2+</sup> ions on the thermal deformation response was evaluated. This was accomplished by calculating the Voronoi volumes of the interlayer atoms and calculating their effective TDCs. Here, it must be noted that it is difficult to capture correlated thermal motions (i.e., of phonons) using Voronoi tessellation, and therefore the TDC of individual atoms may not be accurately evaluated by this approach. However, when applied to a group of neighboring atoms, the temperature dependent Voronoi volume provides qualitatively correct representations of the real TDC. The resulting TDC of the interlayer components calculated in this way is shown as a function of the number of constraints per atom,  $n_c$  in Figure 4b. It is evident that, for flexible networks, that is, with  $n_c < 3$ , the TDC of interlayer water increases with a decrease in  $n_c$ ; in agreement with the enhanced water content, and its confinement in this composition range. This explains why the interlayer water controls the TDC at high Ca/Si compositions. This is intuitively realized when it is seen that the TDC and the density of the interlayer (confined) water are linearly correlated (see Figure 4b inset).

At this point, it is important to note that an increase in the confinement of water with Ca/Si is not simply induced by composition, i.e., an increase in the abundance of strongly hydrophilic Ca-atoms which would enhance the confinement of water. This is because, no such composition linked increase in water confinement is observed for Ca/Si  $\leq$  1.3. Indeed, C–S–H compositions with low Ca/Si feature a highly polymerized and rigid structure. As a result, these systems do not show any relaxation, ensuring that the calcium silicate layers retain a structure that is more similar to the native tobermorite crystal to which they are thought to be related. However, as an increase in the Ca-content progressively depolymerizes the calcium silicate structure, a rigidity transition occurs around Ca/Si  $\approx$  1.5; after which the structure becomes flexible; permitting relaxation and rearrangement. These flexible structures show more “wrinkled” calcium silicate layers (sheets) which are able to increase their area of contact with interlayer water contained between them, thus increasing the level of

water's confinement. In fact, contact is so proximate that interlayer water molecules can transit into the sheets during thermal excitation. It must be noted, however, that the present model of C–S–H tends to produce overly depolymerized calcium silicate structures for high Ca/Si ratios, for example, those featuring  $Q^0$  silicon units that are not observed experimentally. This may result in overestimations of the extent of confinement of water, and in turn, the TDC at high Ca/Si compositions. It is also worth considering that although (water's) confinement increases with Ca/Si, the interlayer spacing of the C–S–H structure also increases. While this may be thought to decrease the extent of nanoscale confinement of water, this is not so, because of the flexible nature of the atomic network, which relaxes, ensuring that in general, the confinement amplifies, resulting in anomalous TDC trends.

#### 4. SUMMARY AND CONCLUSIONS

The role of the atomic network's topology and the confinement of water on thermal deformation behavior of C–S–H have been carefully examined using MD simulation. We note that due to its enhanced TDC, interlayer water contained in C–S–H controls its thermal deformation response. This aspect, however, is sensitive to the confinement of water, which increases with Ca-content for  $\text{Ca/Si} \geq 1.5$ . Using topological constraint theory (TCT), we highlight that C–S–H shows a rigid structure for  $\text{Ca/Si} \leq 1.3$ ; that is, atomic architectures which resist internal relaxations and rearrangements. Since the calcium silicate sheets can maintain their geometry in such more "rigid" systems, the extent of confinement of water and thermal deformations show weak dependence on Ca/Si. For  $\text{Ca/Si} \geq 1.5$ , however, the calcium silicate sheets become increasingly depolymerized and flexible. This allows internal structural relaxations that improve contact, increase proximity, and enhance the solid's interactions with interlayer water. As such, in the flexible domain, the confinement of interlayer water increases sharply with Ca/Si. This results in an anomalous jump in the thermal deformation coefficient (TDC), as C–S–H structures undergo a rigidity transition in this compositional range. Altogether, we find that the nanoconfinement, and in turn the thermal deformation, of water is controlled not just by the composition but also by the topology of the substrate network and the interface as well. New insights into such topology-dependent water confinement and its atomistic origins provide new insight that would be needed to design and synthesize functional construction materials with desirable properties.

#### AUTHOR INFORMATION

##### Corresponding Authors

\*E-mail: [mbauchy@ucla.edu](mailto:mbauchy@ucla.edu).

\*E-mail: [gsant@ucla.edu](mailto:gsant@ucla.edu).

##### ORCID

N. M. Anoop Krishnan: 0000-0003-1500-4947

##### Author Contributions

N.M.A.K. and B.W. contributed equally to this work.

##### Notes

The authors declare no competing financial interest.

#### ACKNOWLEDGMENTS

The authors acknowledge financial support for this research provisioned by: Infravation ERA-NET Plus Grant (31109806.0001), the U.S. Department of Transportation via

the Federal Highway Administration (DTFH61-13-H-00011), U.S. National Science Foundation (CAREER 1253269 and CMMI 1562066), California Energy Commission (Contract PIR 12-032) and Oak Ridge National Laboratory in the form of Laboratory Directed Research and Development (LDRD) support. The contents of this paper reflect the views and opinions of the authors, who are responsible for the accuracy of the datasets presented herein, and do not reflect the views and/or policies of the funding agencies, nor do the contents constitute a specification, a standard or regulation. This research was conducted in the Laboratory for the Chemistry of Construction Materials (LC<sup>2</sup>) and the Laboratory for the Physics of Amorphous and Inorganic Solids (PARISlab) at UCLA. As such, the authors gratefully acknowledge the support that has made these laboratories and their operations possible. This manuscript has been coauthored by ORNL, managed by UT-Battelle LLC under Contract No. DE-AC05-00OR22725 with the U.S. Department of Energy. The publisher, by accepting the article for publication, acknowledges that the U.S. Government retains a nonexclusive, paid-up, irrevocable, worldwide license to publish or reproduce the published form of this manuscript, or allow others to do so, for U.S. Government purposes. The Department of Energy will provide public access to these results of federally sponsored research in accordance with the DOE Public Access Plan (<http://energy.gov/downloads/doe-public-access-plan>).

#### REFERENCES

- (1) Manzano, H.; Moeini, S.; Marinelli, F.; van Duin, A. C. T.; Ulm, F.-J.; Pellenq, R. J.-M. Confined Water Dissociation in Microporous Defective Silicates: Mechanism, Dipole Distribution, and Impact on Substrate Properties. *J. Am. Chem. Soc.* **2012**, *134* (4), 2208–2215.
- (2) Garofalini, S. H.; Mahadevan, T. S.; Xu, S.; Scherer, G. W. Molecular Mechanisms Causing Anomalously High Thermal Expansion of Nanoconfined Water. *ChemPhysChem* **2008**, *9* (14), 1997–2001.
- (3) Qomi, M. J. A.; Bauchy, M.; Ulm, F.-J.; Pellenq, R. J.-M. Anomalous Composition-Dependent Dynamics of Nanoconfined Water in the Interlayer of Disordered Calcium-Silicates. *J. Chem. Phys.* **2014**, *140* (5), 054515.
- (4) Youssef, M.; Pellenq, R. J.-M.; Yildiz, B. Glassy Nature of Water in an Ultraconfining Disordered Material: The Case of Calcium–Silicate–Hydrate. *J. Am. Chem. Soc.* **2011**, *133* (8), 2499–2510.
- (5) Li, Q.; Song, J.; Besenbacher, F.; Dong, M. Two-Dimensional Material Confined Water. *Acc. Chem. Res.* **2015**, *48* (1), 119–127.
- (6) Xu, S.; Scherer, G. W.; Mahadevan, T. S.; Garofalini, S. H. Thermal Expansion of Confined Water. *Langmuir* **2009**, *25* (9), 5076–5083.
- (7) Hu, M.; Goicochea, J. V.; Michel, B.; Poulikakos, D. Water Nanoconfinement Induced Thermal Enhancement at Hydrophilic Quartz Interfaces. *Nano Lett.* **2010**, *10* (1), 279–285.
- (8) Murata, K.; Mitsuoka, K.; Hirai, T.; Walz, T.; Agre, P.; Heymann, J. B.; Engel, A.; Fujiyoshi, Y. Structural Determinants of Water Permeation through Aquaporin-1. *Nature* **2000**, *407* (6804), 599–605.
- (9) Keten, S.; Xu, Z.; Ihle, B.; Buehler, M. J. Nanoconfinement Controls Stiffness, Strength and Mechanical Toughness of [beta]-Sheet Crystals in Silk. *Nat. Mater.* **2010**, *9* (4), 359–367.
- (10) Huck, W. T. Effects of Nanoconfinement on the Morphology and Reactivity of Organic Materials. *Chem. Commun.* **2005**, No. 33, 4143–4148.
- (11) Fichtner, M. Nanoconfinement Effects in Energy Storage Materials. *Phys. Chem. Chem. Phys.* **2011**, *13* (48), 21186–21195.
- (12) Tombari, E.; Salvetti, G.; Ferrari, C.; Johari, G. P. Thermodynamic Functions of Water and Ice Confined to 2nm Radius Pores. *J. Chem. Phys.* **2005**, *122* (10), 104712.

- (13) Ockwig, N. W.; Greathouse, J. A.; Durkin, J. S.; Cygan, R. T.; Daemen, L. L.; Nenoff, T. M. Nanoconfined Water in Magnesium-Rich 2:1 Phyllosilicates. *J. Am. Chem. Soc.* **2009**, *131* (23), 8155–8162.
- (14) Raviv, U.; Laurat, P.; Klein, J. Fluidity of Water Confined to Subnanometre Films. *Nature* **2001**, *413* (6851), 51–54.
- (15) Allen, A. J.; Thomas, J. J.; Jennings, H. M. Composition and Density of Nanoscale Calcium–silicate–hydrate in Cement. *Nat. Mater.* **2007**, *6* (4), 311–316.
- (16) Bullard, J. W.; Jennings, H. M.; Livingston, R. A.; Nonat, A.; Scherer, G. W.; Schweitzer, J. S.; Scrivener, K. L.; Thomas, J. J. Mechanisms of Cement Hydration. *Cem. Concr. Res.* **2011**, *41* (12), 1208–1223.
- (17) Abdolhosseini Qomi, M. J.; Krakowiak, K. J.; Bauchy, M.; Stewart, K. L.; Shahsavari, R.; Jagannathan, D.; Brommer, D. B.; Baronnat, A.; Buehler, M. J.; Yip, S.; Ulm, F.-J.; Van Vliet, K. J.; Pellenq, R. J.-M. Combinatorial Molecular Optimization of Cement Hydrates. *Nat. Commun.* **2014**, *5*, 4960.
- (18) Bauchy, M.; Qomi, M. A.; Ulm, F.-J.; Pellenq, R.-M. Order and Disorder in Calcium–silicate–hydrate. *J. Chem. Phys.* **2014**, *140* (21), 214503.
- (19) Pellenq, R. J.-M.; Kushima, A.; Shahsavari, R.; Van Vliet, K. J.; Buehler, M. J.; Yip, S.; Ulm, F.-J. A Realistic Molecular Model of Cement Hydrates. *Proc. Natl. Acad. Sci. U. S. A.* **2009**, *106* (38), 16102–16107.
- (20) Kovačević, G.; Persson, B.; Nicoleau, L.; Nonat, A.; Veyrazov, V. Atomistic Modeling of Crystal Structure of Ca 1.67 SiH X. *Cem. Concr. Res.* **2015**, *67*, 197–203.
- (21) Richardson, I. G. The Importance of Proper Crystal-Chemical and Geometrical Reasoning Demonstrated Using Layered Single and Double Hydroxides. *Acta Crystallogr., Sect. B: Struct. Sci., Cryst. Eng. Mater.* **2013**, *69* (2), 150–162.
- (22) Scrivener, K. L.; Juilland, P.; Monteiro, P. J. Advances in Understanding Hydration of Portland Cement. *Cem. Concr. Res.* **2015**, *78*, 38–56.
- (23) Pignatelli, I.; Kumar, A.; Alizadeh, R.; Le Pape, Y.; Bauchy, M.; Sant, G. A Dissolution-Precipitation Mechanism Is at the Origin of Concrete Creep in Moist Environments. *J. Chem. Phys.* **2016**, *145* (5), 054701.
- (24) CRC Handbook of Chemistry and Physics, 93rd ed.; CRC: Boca Raton, FL, 2012; <https://www.crcpress.com/CRC-Handbook-of-Chemistry-and-Physics-93rd-Edition/Haynes/p/book/9781439880494> (accessed Aug 23, 2016).
- (25) Plimpton, S. Fast Parallel Algorithms for Short-Range Molecular Dynamics. *J. Comput. Phys.* **1995**, *117* (1), 1–19.
- (26) Shahsavari, R.; Pellenq, R. J.-M.; Ulm, F.-J. Empirical Force Fields for Complex Hydrated Calcium–Silicate Layered Materials. *Phys. Chem. Chem. Phys.* **2011**, *13* (3), 1002–1011.
- (27) Berendsen, H. J. C.; Grigera, J. R.; Straatsma, T. P. The Missing Term in Effective Pair Potentials. *J. Phys. Chem.* **1987**, *91* (24), 6269–6271.
- (28) Fordham, C. J.; Smalley, I. J. A Simple Thermogravimetric Study of Hydrated Cement. *Cem. Concr. Res.* **1985**, *15* (1), 141–144.
- (29) Taylor, H. F. W. *Cement Chemistry*; Thomas Telford, 1997.
- (30) Phillips, J. C. Topology of Covalent Non-Crystalline Solids I: Short-Range Order in Chalcogenide Alloys. *J. Non-Cryst. Solids* **1979**, *34* (2), 153–181.
- (31) Maxwell, J. C. L. On the Calculation of the Equilibrium and Stiffness of Frames. *London Edinb. Dublin Philos. Mag. J. Sci.* **1864**, *27* (182), 294–299.
- (32) Smedskjaer, M. M.; Mauro, J. C.; Yue, Y. Prediction of Glass Hardness Using Temperature-Dependent Constraint Theory. *Phys. Rev. Lett.* **2010**, *105* (11), 115503.
- (33) Mauro, J. C.; Ellison, A. J.; Allan, D. C.; Smedskjaer, M. M. Topological Model for the Viscosity of Multicomponent Glass-Forming Liquids. *Int. J. Appl. Glass Sci.* **2013**, *4* (4), 408–413.
- (34) Bauchy, M.; Qomi, M. J. A.; Bichara, C.; Ulm, F.-J.; Pellenq, R. J.-M. Rigidity Transition in Materials: Hardness Is Driven by Weak Atomic Constraints. *Phys. Rev. Lett.* **2015**, *114* (12), 125502.
- (35) Bauchy, M.; Abdolhosseini Qomi, M. J.; Bichara, C.; Ulm, F.-J.; Pellenq, R. J.-M. Nanoscale Structure of Cement: Viewpoint of Rigidity Theory. *J. Phys. Chem. C* **2014**, *118* (23), 12485–12493.
- (36) Bauchy, M.; Micoulaut, M.; Celino, M.; Le Roux, S.; Boero, M.; Massobrio, C. Angular Rigidity in Tetrahedral Network Glasses with Changing Composition. *Phys. Rev. B: Condens. Matter Mater. Phys.* **2011**, *84* (5), 054201.
- (37) Laurent, O.; Mantsi, B.; Micoulaut, M. Structure and Topology of Soda-Lime Silicate Glasses: Implications for Window Glass. *J. Phys. Chem. B* **2014**, *118* (44), 12750–12762.
- (38) Pelisser, F.; Gleize, P. J. P.; Mikowski, A. Effect of the Ca/Si Molar Ratio on the Micro/nanomechanical Properties of Synthetic C-S-H Measured by Nanoindentation. *J. Phys. Chem. C* **2012**, *116* (32), 17219–17227.
- (39) Manzano, H.; Dolado, J. S.; Ayuela, A. Elastic Properties of the Main Species Present in Portland Cement Pastes. *Acta Mater.* **2009**, *57* (5), 1666–1674.
- (40) Taylor, H. F. W. *Cement Chemistry*; Thomas Telford, 1997.
- (41) Sellevold, E. J.; Bjøntegaard, Ø. Coefficient of Thermal Expansion of Cement Paste and Concrete: Mechanisms of Moisture Interaction. *Mater. Struct.* **2006**, *39* (9), 809–815.
- (42) Shui, Z.; Zhang, R.; Chen, W.; Xuan, D. Effects of Mineral Admixtures on the Thermal Expansion Properties of Hardened Cement Paste. *Constr. Build. Mater.* **2010**, *24* (9), 1761–1767.
- (43) Wang, B.; Cormack, A. N. Molecular Dynamics Simulations of Mg-Doped Beta $\gamma$ -Alumina with Potential Models Fitted for Accurate Structural Response to Thermal Vibrations. *Solid State Ionics* **2014**, *263*, 9–14.
- (44) Shaw, R. The Thermal Expansion of Awillite. *Acta Crystallogr.* **1953**, *6* (5), 428–429.
- (45) Wu, Y.; Tepper, H. L.; Voth, G. A. Flexible Simple Point-Charge Water Model with Improved Liquid-State Properties. *J. Chem. Phys.* **2006**, *124* (2), 024503.
- (46) Sun Lee, W.; Yu, J. Comparative Study of Thermally Conductive Fillers in Underfill for the Electronic Components. *Diamond Relat. Mater.* **2005**, *14* (10), 1647–1653.
- (47) Xu, H.; Zhao, Y.; Vogel, S. C.; Daemen, L. L.; Hickmott, D. D. Anisotropic Thermal Expansion and Hydrogen Bonding Behavior of Portlandite: A High-Temperature Neutron Diffraction Study. *J. Solid State Chem.* **2007**, *180* (4), 1519–1525.
- (48) De Almeida, M.; Brook, R. J.; Carruthers, T. G. Thermal Expansion of Ceramics in the MgO–CaO System. *J. Mater. Sci.* **1979**, *14* (9), 2191–2194.
- (49) Vegard, L. Die Konstitution der Mischkristalle und die Raumfüllung der Atome. *Eur. Phys. J. A* **1921**, *5* (1), 17–26.
- (50) Nonat, A. The Structure and Stoichiometry of C-S-H. *Cem. Concr. Res.* **2004**, *34* (9), 1521–1528.
- (51) Raki, L.; Beaudoin, J.; Alizadeh, R.; Makar, J.; Sato, T. Cement and Concrete Nanoscience and Nanotechnology. *Materials* **2010**, *3* (2), 918–942.
- (52) Selvam, R. P.; Subramani, V. J.; Murray, S.; Hall, K. D. *Potential Application of Nanotechnology on Cement Based Materials*, Final Report MBTC DOT 2095/3004; National Technical Information Service: Alexandria, VA, 2009.